IEEE Photonics Journal
An IEEE Photonics Society Publication

Modeling and Analysis of BER Performance in a SPAD-Based Integrated Fiber Optical Receiver

Volume 10, Number 6, December 2018

Hiwa Mahmoudi
Michael Hofbauer, *Member, IEEE*
Bernhard Steindl
Kerstin Schneider-Hornstein
Horst Zimmermann, *Senior Member, IEEE*

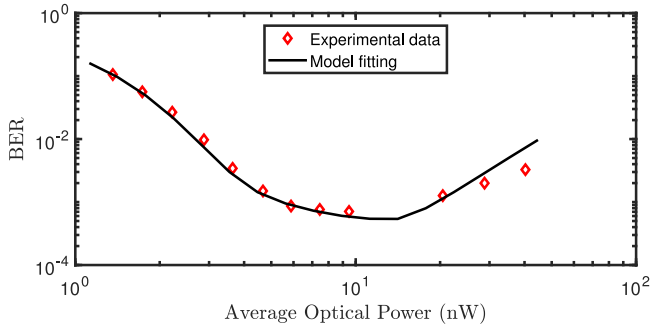

DOI: 10.1109/JPHOT.2018.2875519
1943-0655 © 2018 CCBY

Modeling and Analysis of BER Performance in a SPAD-Based Integrated Fiber Optical Receiver

Hiwa Mahmoudi, Michael Hofbauer, *Member, IEEE*, Bernhard Steindl, Kerstin Schneider-Hornstein, and Horst Zimmermann, *Senior Member, IEEE*

Institute of Electrodynamics, Microwave and Circuit Engineering, Technische Universität Wien, Gusshausstraße 25/354, 1040, Vienna, Austria

DOI:10.1109/JPHOT.2018.2875519

Manuscript received August 14, 2018; revised September 28, 2018; accepted October 7, 2018. Date of publication October 11, 2018; date of current version October 25, 2018. This work was supported by the Austrian Science Fund (FWF) under Grant P28335-N30. Corresponding author: Hiwa Mahmoudi (e-mail: hiwa.mahmoudi@tuwien.ac.at).

Abstract: An analytical approach to model and analysis of the bit-error ratio (BER) performance in multi-single photon avalanche diode (SPAD) optical receivers is presented. The model covers all important non-ideality effects including the detector dead time, the optical signal profile, and the SPAD intrinsic parasitics. This is very helpful to understand the bottlenecks that limit the performance and, therefore, is critical to attempt further improvements. A good agreement to the experimental data is achieved and it is found that the crosstalk makes the major contribution to the BER as compared to the other parasitic effects including dark-counts and afterpulsing.

Index Terms: Bit-error ratio (BER), crosstalk, detector dead time, single-photon avalanche diode (SPAD), optical receiver.

1. Introduction

1.1 Background

The advantage of integration within CMOS technology and the ability to generate a detectable signal in response to a single photon event have made the single photon avalanche diode (SPAD) a very attractive candidate as photodetector [1]–[6]. Recently, it has been shown that in optical receiver applications, a well-designed SPAD receiver using an array of few SPADs can bring significant sensitivity improvements [6], [7] as compared to the avalanche photo-diode (APD) in the linear mode, which is susceptible to excess and circuit noise.

A first-order performance analysis of SPAD arrays can be found in [8], [9]. However, a careful design of a highly sensitive optical receiver requires a thorough understanding of SPAD non-ideality effects. These effects can make the SPAD blind to photons (due to detector dead time) or fire avalanche events without a photon being absorbed (due to parasitic effects) and may significantly degrade the receiver performance. In [10], we presented a statistical and experimental study of SPAD parasitics and it was shown that the Bit-error ratio (BER) performance of a single-SPAD receiver is considerably degraded due to a high avalanche probability imposed by these effects.

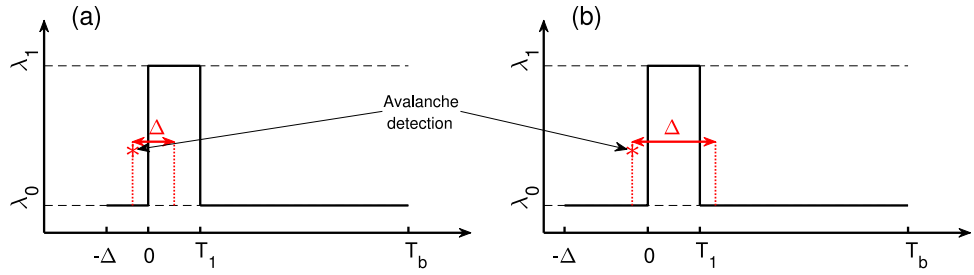

Fig. 1. Maximum photo-count rate corresponding to the incident signal during a '1' bit with an RZ profile. Due to the dead time Δ, a late avalanche detection within the previous bit time (caused by λ_0) can significantly increase the error probability in the current bit (0, T_b).

To provide an acceptable BER, one solution is to use a photon counting scheme in the single-SPAD receiver, where an avalanche counting threshold is defined for logical decision-making [11]. This improves the BER performance significantly as the error probability decreases exponentially with the counting threshold. However, as a bit time should be long enough to cover several detector dead times, it exhibits a lower bit rate. Another solution is to use multi-SPAD structures to realize a faster receiver at the expense of reduced fill-factor. In fact, in an array of SPADs a decision-making threshold can be defined on the number of SPADs triggered during each bit time. An experimental demonstration of such a receiver is presented in [6], where an array of four SPADs is employed to achieve an acceptable BER (smaller than 2×10^{-3}). Due to the parallel operation of SPADs, the multi-SPAD receiver can exhibit higher data rates as compared to the single-SPAD counterpart.

In order to determine the contribution of different parasitics to the BER and to identify the most limiting effect for further optimizations, a BER model of the multi-SPAD optical receiver is required. Unfortunately, the model presented in [11] is applicable only to the single-SPAD receiver and doesn't include the crosstalk effect, which can significantly degrade the performance of the multi-SPAD structure as it will be shown later. Therefore, this work presents a comprehensive model for BER performance in the multi-SPAD optical receivers to take all important non-ideality effects into account. These effects comprise the dead time, the light source extinction ratio that considerably affects the photon counting statistics, and the parasitic effects, which increase the error probability by triggering avalanche detections without photon absorption. Furthermore, the presented model successfully covers the return to zero (RZ) optical signal profile, which can provide a better performance than non-return to zero (NRZ) [6].

1.2 Operating Principles and Modeling Considerations

To transmit a logical '1', the light source is turned on to impose a (maximum) photo-count rate defined as $\lambda_1 = \eta I_{op}$ (measured in photons per second). Here, η is a coefficient (in photons per joule) and expresses the total detection efficiency of the SPAD and I_{op} is the optical power of the incident signal (in watts).

The incident signal may have an RZ or NRZ profile. The maximum photo-count rate corresponds to a zero detector dead time (denoted here as Δ). In practice, the dead time is non-zero and comprises the avalanche quenching time, required to decrease the reverse-bias voltage on the SPAD below the breakdown voltage, and the recovery time, required to restore the bias voltage to above the SPAD's breakdown voltage and make it ready for the next detection. In addition, Δ may include a hold-off time before the recovery in order to reduce the afterpulsing probability. In fact, the afterpulsing probability decreases exponentially with time delay as is explained later. A long Δ, however, can significantly degrade the receiver performance, especially when it is comparable to the optical pulse width (i.e. T_1 during which the light source is turned on to transmit a logical '1' as shown in Fig. 1).

Although the light source is turned off within a '0' bit, there is a non-zero photo-count rate ($\lambda_0 = \lambda_1/k_{ex}$) due to the limited extinction ratio ($k_{ex} < \infty$) of the light source. This acts as a background

noise in the fiber optical receiver [6] and may increase the error probability corresponding to '0' bits. Therefore, this effect has to be taken into account in the BER modeling as well.

In addition to the above mentioned issues, the SPAD intrinsic parasitics including dark-count, afterpulsing, and crosstalk can dramatically affect its performance [12], [13]. In dark condition, the thermally or tunneling generated carriers produce a detection rate called "dark-count" rate (r_{dc}), which is generally in the range of Hz to MHz. Many CMOS-integrated SPADs, however, exhibit dark-count rates in the higher part of this range. Furthermore, the release of trapped carriers yields in an avalanche mechanism exhibiting strong correlation to previous avalanche detections. This is called "afterpulsing" and usually shows a delay in the nanosecond range. The optical interaction between the SPADs refers to "crosstalk", which is an avalanche triggered by photons emitted from hot-carriers in another SPAD where an avalanche has just been fired. Moreover, the diffusion of optically generated carriers somewhere else in the bulk can cause a "delayed" crosstalk as is explained later. These parasitic effects can result in making wrong decisions in the SPAD receiver. For example, a high crosstalk probability can result in triggering a majority of SPADs within a certain bit time and, consequently, deciding for a logical '1' while a '0' bit has been transmitted. High crosstalk probability can also result in making a wrong decision for logical '1' ('0' is detected instead of '1'), when it triggers a group of SPADs late within the previous bit time (e.g. in Fig. 1) and make the SPADs blind during the whole or a part of the interval $(0, T_1)$. In the next section, all the above mentioned effects are considered and included in the BER model to enable an accurate analysis and design of the multi-SPAD receiver.

2. BER Modeling Procedure

The BER performance of a receiver can be modeled as the probability of making a wrong decision (error) corresponding to '1' and '0' bits. In the multi-SPAD receiver (comprising an array of n_s SPADs), a decision is made by comparing the number of SPADs triggered within a given bit to a decision threshold (n_{th}). Therefore, the BER performance can be defined as

$$\begin{aligned} P_e &= P_e(\text{'1'}) + P_e(\text{'0'}) \\ &= \sum_{i_t=0}^{n_{th}-1} P_t(i_t|\text{'1'})P_b(\text{'1'}) + \sum_{i_t=n_{th}}^{n_s} P_t(i_t|\text{'0'})P_b(\text{'0'}) \\ &= \frac{1}{2}\left[\sum_{i_t=0}^{n_{th}-1} P_t(i_t|\text{'1'}) + \sum_{i_t=n_{th}}^{n_s} P_t(i_t|\text{'0'})\right] \end{aligned} \tag{1}$$

where $P_e(\text{'1'})$ and $P_e(\text{'0'})$ represent the error probabilities for '1' and '0' bits, respectively. $P_b(\text{'1'})$ and $P_b(\text{'0'})$ are the probabilities of receiving logical '1' and '0' and are equal to 0.5 for equally likely bits. $P_t(i_t|\text{'b'})$ denotes the probability that i_t different SPADs (channels) trigger an avalanche (due to photon detection or parasitics) during the same bit time, given the logic bit 'b' (can be '1' or '0'). A decision for '1' is made, when at least n_{th} SPADs are triggered within a bit time ($i_t \geq n_{th}$). Conversely, if $i_t < n_{th}$ the received bit is decided as a '0'. Our experimental investigation on a 4-SPAD receiver ($n_s = 4$) shows that $n_{th} = 4$ can overcome the parasitic effects to provide an acceptable BER.

According to (1), BER is successfully modeled if we obtain $P_t(i_t|\text{'b'})$ for all i_t, given '1' and '0'. However, avalanche detections in i_t different SPADs during a bit time can be caused by photons or any type of parasitics. Therefore, in order to obtain $P_t(i_t|\text{'b'})$, all possible combinations of triggering SPADs due to different mechanisms are included as

$$P_t(i_t|\text{'b'}) = \sum_{i_p=0}^{i_t} \sum_{i_d=0}^{i_t-i_p} \sum_{i_a=0}^{i_t-i_p-i_d} P(i_p, i_d, i_a, i_c|\text{'b'}), \tag{2}$$

where $i_p + i_d + i_a + i_c = i_t$ and i_p, i_d, i_a, and i_c indicate the number of SPADs triggered due to photon absorption, dark-count, afterpulsing, and crosstalk, respectively. Now, the chain rule

enables the joint probability $P(i_p, i_d, i_a, i_c|\text{'b'})$ to be calculated as the product of conditional probability distributions over the photon statistics for given optical signals ('1' and '0') and the SPAD parasitics as

$$\begin{aligned} P(i_p, i_d, i_a, i_c|\text{'b'}) &= P_p(i_p|\text{'b'})P_d(i_d|i_p, \text{'b'})P_a(i_a|i_p, i_d, \text{'b'})P_c(i_c|i_p, i_d, i_a, \text{'b'}) \\ &= P_p(i_p|\text{'b'})P_d(i_d|i_p)P_a(i_a|i_p + i_d)P_c(i_c|i_p + i_d + i_a) \end{aligned} \tag{3}$$

Here, the SPAD intrinsic parasitics (i.e. P_d, P_a, P_c) are supposed to be independent of the optical signal ('b'), which is a reasonable assumption. In other words, the avalanche probability due to the parasitics in an available SPAD (i.e. not triggered by the optical signal within a given bit time) doesn't depend on the current incident optical power. Furthermore, to obtain the conditional probabilities, only the number of triggered and untriggered (available) SPADs are important, i.e. it doesn't matter which mechanism has fired an avalanche in a triggered SPADs. For example, $P_a(1|2)$ expresses the probability of afterpulse in one ($i_a = 1$) SPAD, when two other SPADs are already triggered. In fact, both triggered SPADs may have been triggered through photon absorption ($i_p = 2, i_d = 0$) or dark-count ($i_p = 0, i_d = 2$), or one by photon absorption and one by dark-count ($i_p = 1, i_d = 1$).

The conditional probabilities on the right hand side of (3) need to be accurately evaluated as each avalanche mechanism imposes its own features and complexity. In the following sections, it is explained how these conditional SPAD's avalanche detection probabilities corresponding to photon absorption (P_p), dark-count (P_d), afterpulsing (P_a), and crosstalk (P_c) mechanisms can be calculated.

2.1 Photon Absorption in Presence of Detector Dead Time

The probability that i_p (out of n_s) SPADs are triggered by photon absorption during a given bit time can be obtained as

$$P_p(i_p|\text{'b'}) = C(n_s, i_p)\,[p_{nz}(\text{'b'})]^{i_p}\,[p_z(\text{'b'})]^{(n_s - i_p)}, \tag{4}$$

where $C(n_s, i_p) = n_s!/[i_p!(n_s - i_p)!]$ represents the number of possible combinations that i_p (among n_s available) SPADs trigger. The symbols p_{nz}('b') and p_z('b') denote the probabilities that a SPAD exhibits a non-zero (at least one) or a zero photo-count within the bit time of the received signal 'b'. Furthermore, it is clear that

$$p_{nz} = 1 - p_z. \tag{5}$$

The photon arrivals can be modeled as Poisson process [14]. Therefore, the waiting time between subsequent arrivals exhibits an exponential distribution and is a memoryless process. It can be shown that in a Poisson process with an average rate of λ, the probability that no (zero) event occurs within a time interval T is given by $p_z = e^{-\lambda T}$. Consequently, according to (5), the probability that at least one (non-zero) event occurs can be obtained as $p_{nz} = 1 - e^{-\lambda T}$. Furthermore, the corresponding probability distribution function (over time) is given by $\lambda e^{-\lambda t}$. These basic equations will be used to model the profile of the incident optical signal corresponding to logical '1' and '0' and derive p_z and p_{nz} for different optical signals ('b'). Furthermore, as the detector dead time is comparable to the bit time (both are in the nanosecond range) and essentially affects the photo-count statistics [14], it has to be taken into consideration.

2.1.1 Photo-Count Statistics for Logical '0': Although the light source is turned off during a '0' bit, an average optical signal corresponding to λ_0 is assumed due to the limited extinction ratio. The SPAD can be available to detect a photon either within the whole bit time $(0, T_b)$ or only within $(\tau + \Delta, T_b)$ due to a possible photo-count in the previous bit within $\tau \in (-\Delta, 0)$. Therefore, the

probability that the SPAD counts no photon in the current bit is given by

$$\begin{aligned} P_z(\text{'0'}) &= e^{-\lambda_0 T_b} e^{-\lambda_0 \Delta} + \int_{-\Delta}^{0} e^{-\lambda_0 [T_b - (\tau+\Delta)]} \lambda_0 e^{-\lambda_0 [\tau+\Delta]} d\tau \\ &= e^{-\lambda_0 T_b} e^{-\lambda_0 \Delta} + \lambda_0 \Delta e^{-\lambda_0 T_b} = \left(e^{-\lambda_0 \Delta} + \lambda_0 \Delta\right) e^{-\lambda_0 T_b} \\ &\simeq \left(1 + \frac{(\lambda_0 \Delta)^2}{2}\right) e^{-\lambda_0 T_b} \end{aligned} \tag{6}$$

Here, the term $e^{-\lambda_0 \Delta}$ stands for the probability of having no photo-count in the previous bit within $\tau \in (-\Delta, 0)$. Although, the previous bit can be a logical '1' or '0', an optical signal of λ_0 is supposed and this implicitly assumes an RZ profile for the logical '1'. In fact, the RZ profile is more interesting in our analyzes as it shows a better receiver performance. This has been verified by our experiments and will be explained later. Nevertheless, the equation corresponding to an NRZ profile can also be derived in a similar manner. Now, to have all terms required in (4), $P_{nz}(\text{'0'})$ can be simply obtained according to (5) and (6).

Intuitively, the probability of having SPAD blind for a while at the beginning of the '0' bit time increases the chance that no photon is counted and results in a reduced error probability. This effect (i.e. $\Delta \neq 0$) corresponds to the term $(\lambda_0 \Delta)^2/2$ in (6), which is seemingly an improvement. However, it is, and must be, negligible ($\lambda_0 \Delta \ll 1$). Otherwise, a considerable $\lambda_0 \Delta$ will cause a large $\lambda_0 T_b$ as $T_b > \Delta$ and this results in a high probability to detect a photon within $(\tau + \Delta, T_b)$ which is undesirable. Therefore, the effect of Δ cannot be significant for '0' bits. Conversely, it strongly affects the photo-count properties of the SPAD for '1' bits as is shown in the following.

2.1.2 Photo-Count Statistics for Logical '1': For a logical '1', we assume an optical signal corresponding to the RZ profile shown in Fig. 1, where the light source is turned on for $(0, T_1)$. The photo-count statistics are more complex to derive as compared to a NRZ signal ($T_1 = T_b$), however, the RZ profile ($T_1 < T_b$) shows lower error probabilities due to a decrease in the parasitic effects. In fact, according to our experimental results [10], the afterpulsing and crosstalk probabilities decrease exponentially with time delay. Therefore, as the RZ profile of logical '1' concentrates the photon detection within $(0, T_1)$, it enforce a delay between the detections in the current bit time and the next bit time (i.e. $(T_b, 2T_b)$) to reduce the chance that an afterpulse or delayed crosstalk triggers within the next bit time. This reduces the probability to make a wrong decision regarding the next bit, especially if it is a logical '0'.

If the SPAD is available within the whole bit time $(0, T_b)$, the probability that no photon is detected is given by the product of three terms corresponding to having no detection in the intervals of $(0, T_1)$, (T_1, T_b), and $(-\Delta, 0)$, where the average detection in the first interval is equal to λ_1 and in the last to intervals is equal to λ_0 (see Fig. 1). This probability is obtained as the first term in the right hand side of the following equation. However, as $\Delta \neq 0$, it is possible that there is a detection within $(-\Delta, 0)$ and this can dramatically increase the error probability ($P_z(\text{'1'})$) in the current '1' bit as it blinds the detector to the incident photons (equivalent to λ_1). The corresponding probability can be calculated by an integration over the interval $(-\Delta, 0)$ as it follows.

$$P_z(\text{'1'}) = \left(e^{-\lambda_1 T_1} e^{-\lambda_0 [T_b - T_1]}\right) e^{-\lambda_0 \Delta} + \int_{-\Delta}^{0} p_z(\text{'1'}, \tau) d\tau, \tag{7}$$

where, $p_z(\text{'1'}, \tau)$ is a probability density function, which depends on the relative values of Δ and T_1. In fact, we have

- for $T_1 \geq \Delta$:

$$p_z(\text{'1'}, \tau) = \left(e^{-\lambda_1 [T_1 - (\tau+\Delta)]} e^{-\lambda_0 [T_b - T_1]}\right) \lambda_0 e^{-\lambda_0 [\tau+\Delta]}, \tag{8}$$

and accordingly, the integral term in (7) is obtained as

$$\int_{-\Delta}^{0} p_z(\text{'1'}, \tau) d\tau = \frac{\lambda_0}{\lambda_1 - \lambda_0} e^{-\lambda_1 [T_1 - \Delta]} e^{-\lambda_0 [T_b - (T_1 - \Delta)]} \left(1 - e^{-[\lambda_1 - \lambda_0]\Delta}\right), \tag{9}$$

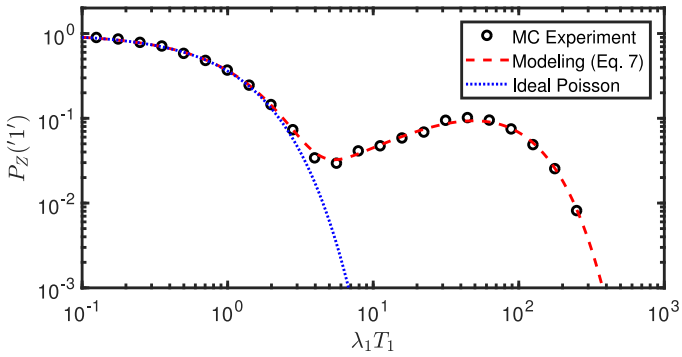

Fig. 2. The error probability corresponding to logical '1' as a function of $\lambda_1 T_1$ obtained by different approaches (Monte Carlo experiment, presented modeling based on (7), and ideal Poisson model) for $\Delta/T_b = 0.4$, $T_1/T_b = 0.2$, and $k_{ex} = 200$.

- and for $T_1 < \Delta$:

$$p_z('1', \tau) = \begin{cases} \left(e^{-\lambda_1[T_1-(\tau+\Delta)]}e^{-\lambda_0[T_b-T_1]}\right)\lambda_0 e^{-\lambda_0[\tau+\Delta]}, & -\Delta < \tau < -\Delta + T_1 \\ \left(e^{-\lambda_0[T_b-(\tau+\Delta)]}\right)\lambda_0 e^{-\lambda_0[\tau+\Delta-T_1]}, & -\Delta + T_1 < \tau < 0 \end{cases}, \tag{10}$$

and as a result, the integral term in (7) is obtained as

$$\int_{-\Delta}^{0} p_z('1', \tau)d\tau = \lambda_0 e^{-\lambda_0[T_b-T_1]}\left(\frac{e^{-\lambda_0 T_1} - e^{-\lambda_1 T_1}}{\lambda_1 - \lambda_0} + (\Delta - T_1)\right). \tag{11}$$

In order to verify the developed model for $P_z('1')$, a Monte Carlo (MC) experiment is implemented to measure the error probability (i.e. the probability of no photon count for '1' bits). In this experiment, 10^4 equally likely '1' and '0' bits are generated and photon arrivals are assigned by drawing random numbers from exponential distributions corresponding to λ_1 and $\lambda_0 = \lambda_1/k_{ex}$, to simulate the on and off states of the light source, respectively. Then, if the SPAD is available, a simulate photon detection is counted within the corresponding bit and, consequently, the SPAD is supposed as unavailable (dead) for a time duration equal to Δ. As a result, a photon arrived within this dead time will not be counted. It has to be noted that here, the extinction ratio of the light source is assumed as $k_{ex} = 200$, which is a realistic value according to our experimental investigation.

Fig. 2 compares the obtained results based on the Monte Carlo experiment, the developed model in this section, and an ideal Poisson model where the effect of Δ is not considered ($\Delta = 0$). This figure demonstrates that the model based on equations (7)–(11) captures the photo-count statistics very well and can be reliably used to model the receiver BER. It also provides more insight into how the error probability can be minimized by optical signal profile. In fact, it shows that at lower optical powers ($\lambda_1 T_1 < 4$), the error probability decreases exponentially with $\lambda_1 T_1$. At higher optical powers ($\lambda_1 T_1 > 6$), the error probability increases again. The reason is that the effect of λ_0 due to the limited extinction ratio, which becomes significant, i.e. there is a considerable chance that a photon is counted late in the previous bit time (within $(-\Delta, 0)$) and the SPAD gets blind for the photons arriving due to $\lambda_1 T_1$ and transmitting a logical '1'. At very high optical powers ($\lambda_1 T_1 > 100$), the error probability decreases exponentially again, and this is due to a high chance for photon counting within a '1' bit, even when the SPAD has been blind over the interval $(0, T_1)$. In fact, λ_1, and accordingly, λ_0 is so high that most probably a photon will be counted within (T_1, T), although the light source is turned off. Unfortunately, for the same reason, there will be a very high error probability for '0' bits at such high optical power and, therefore, the receiver cannot operate as it sees almost every bit as a logical '1'. Therefore, from a BER performance point of view in this specific example, the optimized signal intensity corresponds to $\lambda_1 T_1$ of around 5, where total error probabilities are minimized.

2.2 Intrinsic Parasitic Effects

In the previous section, we derived the photo-count statistics to obtain the first conditional probability term on the right hand side of (3). The other three terms $P_{\rm d}(i_{\rm d}|i_{\rm p})$, $P_{\rm a}(i_{\rm a}|i_{\rm p}+i_{\rm d})$, and $P_{\rm c}(i_{\rm c}|i_{\rm p}+i_{\rm d}+i_{\rm a})$ correspond to the intrinsic parasitic effects and are obtained in this section.

2.2.1 Dark-Count: Similar to the photo-count statistics, one can assume that the dark-count in an available SPAD is independent of the dark-count in the other SPADs. Furthermore, we can suppose that the dark-count is a Bernoulli process, where within a given bit time, an avalanche is triggered in a SPAD or not with a probability of $p_{\rm d}$ or $1-p_{\rm d}$, respectively. Therefore, the conditional dark-count probability is expressed as the product of probabilities for each available SPAD given as

$$P_{\rm d}(i_{\rm d}|i_{\rm p}) = C(n_{\rm s}-i_{\rm p}, i_{\rm d})(p_{\rm d})^{i_{\rm d}}(1-p_{\rm d})^{(n_{\rm s}-i_{\rm p}-i_{\rm d})}. \tag{12}$$

Here, $P_{\rm d}(i_{\rm d}|i_{\rm p})$ is the probability that $i_{\rm d}$ (out of $n_{\rm s}-n_{\rm p}$) SPADs are triggered through photo-count during a given bit time and $C(n_{\rm s}-n_{\rm p}, i_{\rm d}) = (n_{\rm s}-n_{\rm p})!/[i_{\rm d}!(n_{\rm s}-n_{\rm p}-i_{\rm d})!]$ representing the number of possible combinations that $i_{\rm d}$ SPADs trigger.

Now, we have to obtain $p_{\rm d}$ and $p_{\rm a}$ corresponding to the dark-count and afterpulsing probabilities for one SPAD within a bit time. The dark-count process shows an exponential distribution over time, which is a memoryless distribution [10]. Furthermore, the dark-count rate ($r_{\rm d}$ denoting the number of dark-counts in one second) is typically in the sub-MHz range [10]. It increases with the SPAD excess bias voltage, however, is still around three orders of magnitude smaller than the operating bit rate (50–100 Mbit/s). As a result, $p_{\rm d}$ can be obtained as

$$p_{\rm d} \simeq \int_0^{T_{\rm b}} \frac{1}{\tau_{\rm d}} e^{-t/\tau_{\rm d}} dt \simeq 1 - e^{-T_{\rm b}/\tau_{\rm d}} \simeq 1 - \left(1 - \frac{T_{\rm b}}{\tau_{\rm d}}\right) \simeq \frac{T_{\rm b}}{\tau_{\rm d}}, \tag{13}$$

where $\tau_{\rm d} = 1/r_{\rm d}$ is the dark-count time constant and we have $\tau_{\rm d} \gg T_{\rm b}$. This approximation is remarkably accurate and has been experimentally proven in our previous work [10].

2.2.2 Afterpulsing: Like $P_{\rm d}(i_{\rm d}|i_{\rm p})$, in order to obtain $P_{\rm a}(i_{\rm a}|i_{\rm p}+i_{\rm d})$ within the corresponding bit time, where $i_{\rm p}+i_{\rm d}$ SPADs have been already triggered through photo-count and dark-count processes, we have

$$P_{\rm a}(i_{\rm a}|i_{\rm p}+i_{\rm d}) = C(n_{\rm s}-i_{\rm p}-i_{\rm d}, i_{\rm a})(p_{\rm a})^{i_{\rm a}}(1-p_{\rm a})^{(n_{\rm s}-i_{\rm p}-i_{\rm d}-i_{\rm a})}. \tag{14}$$

The afterpulsing probability $p_{\rm a}$, however, cannot be derived based on the same approximation as in (13). In fact, the afterpulsing time constant ($\tau_{\rm a}$) is in the nanosecond range, and therefore, is comparable to the bit time as well as the quencher dead time. In addition, it is strongly correlated to the previous avalanche detections. As a result, we need a more accurate model and first derive $p_{\rm a}^*$ as the probability of having an afterpulse within a bit time (Δ^*, $\Delta^*+T_{\rm b}$), when there is a time delay of Δ^* between the last avalanche detection triggered at $t=0$.

$$p_{\rm a}^* = A_0 \int_{\Delta^*}^{\Delta^*+T_{\rm b}} \frac{1}{\tau_{\rm a}} e^{-t/\tau_{\rm a}} dt = A_0 e^{-\Delta^*/\tau_{\rm a}} \left(1 - e^{-T_{\rm b}/\tau_{\rm a}}\right). \tag{15}$$

Here, A_0 denotes the total afterpulsing probability, i.e. $A_0 = p_{\rm a}^*$ for $\Delta^* = 0$ and $T_{\rm b} = \infty$. A_0 is a constant that includes the number of traps depending on the quencher dead time. In fact, the avalanche is a random process and, accordingly, there is an uncertainty in the number of traps. However, as the active quencher shows a fixed Δ, there is a certain number of average traps per avalanche which is included in A_0. This constant can be measured using the SPAD dark noise statistics, as it is explained in [10]. In (15), the term $e^{-\Delta^*/\tau_{\rm a}}$ demonstrates that the afterpulsing probability exponentially decreases with the time delay between the last afterpulse and the corresponding bit time. We believe, this is a major reason behind the superior receiver performance when RZ optical signal is used as compared to NRZ. In fact, the RZ profile provides a time gap between photo-count moment (within '1' bit) and the next bit time and reduces the afterpulsing effect significantly.

It is important to note that one cannot use $p_{\rm a}^*$ as the afterpulsing probability in the receiver operation mode as we do not know the time delay between the last avalanche and the corresponding bit. Therefore, we have to estimate the (average) time delay between an avalanche moment and the

TABLE 1
Conditional Crosstalk Probabilities as a Function of the Average One-to-One Crosstalk Probability ($\tilde{p}_c$)

$P_c(0\|0) = 1$ $P_c(k\|0) = 0,\ k \in \{1,2,3,4\}$	$P_c(0\|2) = (1-\tilde{p}_c)^4$ $P_c(1\|2) = 2\left(1-(1-\tilde{p}_c)^2\right)(1-\tilde{p}_c)^3$
$P_c(0\|1) = (1-\tilde{p}_c)^3$ $P_c(1\|1) = 3\tilde{p}_c(1-\tilde{p}_c)^2(1-\tilde{p}_c)^2$	$P_c(2\|2) = \left(2\tilde{p}_c - \tilde{p}_c^2\right)^2$ $+ 2\left(2\,\tilde{p}_c - \tilde{p}_c^2\right)\tilde{p}_c(1-\tilde{p}_c)^2$
$P_c(2\|1) = 3\tilde{p}_c^2(1-\tilde{p}_c)^3 + 6\tilde{p}_c^2(1-\tilde{p}_c)^4$ $P_c(3\|1) = \tilde{p}_c^3 + 3\tilde{p}_c^2(1-\tilde{p}_c)\left(1-(1-\tilde{p}_c)^2\right)$ $+ 3\tilde{p}_c(1-\tilde{p}_c)^2\left(\tilde{p}_c^2 + 2\tilde{p}_c^2(1-\tilde{p}_c)\right)$	$P_c(0\|3) = (1-\tilde{p}_c)^3$ $P_c(1\|3) = 1-(1-\tilde{p}_c)^3$ $P_c(0\|4) = 1$

next bit time. First of all, we suppose that the receiver has an acceptable performance. This means the majority of avalanche detections are caused by photo-count in '1' bits (i.e. when the optical source is turned on). As a result, ignoring the secondary effects that may cause an avalanche is a reasonable assumption and one can assume that the last avalanche moment is within the interval $(0, T_1)$ of the last '1' bit. Accordingly, the afterpulsing probability in the receiver operating mode (receiving a sequence of '1' and '0' bits) can be estimated as

$$\begin{aligned} p_a &\simeq P(1)p_a^* + P(\text{'0'})p_a^*[e^{-T_b/\tau_a}P(\text{'1'}) + P(\text{'0'})[e^{-T_b/\tau_a}P(\text{'1'}) + P(\text{'0'})[... \\ &\simeq \frac{1}{2}p_a^* + \frac{1}{2}p_a^*\left[\frac{1}{2}e^{-T_b/\tau_a} + \frac{1}{2}\left[\frac{1}{2}e^{-T_b/\tau_a} + \frac{1}{2}\left[\frac{1}{2}e^{-T_b/\tau_a}\ ...\right.\right.\right. \\ &\simeq p_a^*\left(\frac{1+e^{-T_b/\tau_a}}{2}\right) \simeq A_0 e^{-\Delta^*/\tau_a}\left(\frac{1-e^{-2T_b/\tau_a}}{2}\right). \end{aligned} \tag{16}$$

Here, Δ^* is equal to $(T_b - T_1/2)$ denoting the minimum time delay between the last avalanche moment and the current bit time. It is important to note that the last avalanche moment is approximated as the middle point of the interval $(0, T_1)$ within the previous bit which has been a '1' bit. This implicitly supposes that $T_b - T_1/2$ is longer than the quencher dead time (Δ). Otherwise, we set $\Delta^* = \Delta$. However, if the previous bit has been a '0' bit, the afterpulsing probability decreases by, at least, an exponential term of e^{-T_b/τ_a} due to a longer time delay to the last avalanche detection.

2.2.3 Crosstalk: In our previous work [10], we presented a crosstalk modeling approach in a multi-SPAD receiver, which was verified by experimental data. Here, we refer to this model summarized in the following.

It has been shown that the average SPAD-to-SPAD (one-to-one) crosstalk probability ($\tilde{p}_c$) is dominated by a "delayed" crosstalk mechanism due to the diffusion of optically generated carriers in the bulk. The crosstalk probability increases with the excess bias voltage and shows an average delay of a few nanoseconds (~3 ns). In order to model the conditional crosstalk probabilities ($P_c(i_c|i_p + i_d + i_a)$ in (3), crosstalk is assumed as a Bernoulli process. Furthermore, cascading crosstalks are taken into account, where a crosstalk-triggered avalanche may trigger a following avalanche in another available SPAD in the array.

As an example, in an array of four SPADs, $P_c(1|1)$ represents the probability of triggering one ($i_c = 1$) SPAD (out of the three available SPADs) due to crosstalk, when initially only one SPAD ($i_p + i_d + i_a = 1$) has been triggered.

$$P_c(1|1) = \left[3\tilde{p}_c(1-\tilde{p}_c)^2\right]\left[(1-\tilde{p}_c)^2\right]. \tag{17}$$

Here, the terms inside the first square bracket determine the probability that (only) one SPAD triggers and the second bracket denotes the probability that this SPAD doesn't trigger the other two SPADs. Finally, Table 1 contains all required P_c combinations for $n_s = 4$ to complete the BER model presented in this section.

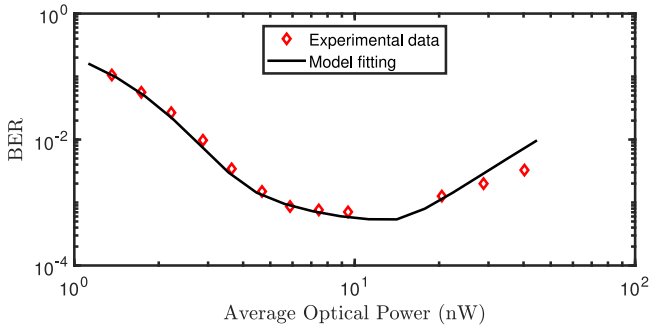

Fig. 3. Measured and model fitting results of the BER performance for the multi-SPAD receiver presented in [6] at a data rate of 50 Mbit/s. Here the optical power of 10nW is equivalent to $\sim 3.2 \times 10^{10}$ photons per second (corresponding to the 635nm light source used in our experiment), which means an average of ~640 photons per bit at 50 Mbit/s.

3. Results and Discussion

In Section 2, we developed a BER model for the multi-SPAD receiver, which includes the intrinsic parasitic effects as well as the photon-count statistics corresponding to a return to zero optical signal in presence of the detector dead time. The dead time duration and the avalanche probabilities of different parasitics (as a function of the excess bias voltage) are obtained using the characterization approach presented in [10] based on dark noise experimental measurements. Therefore, to obtain the BER value at given optical power, bit rate, and excess bias voltage values, all required model parameters (used in the above-described equations) are known or experimentally obtained except λ_1, which is a function of the detection efficiency of the SPAD (η) and the incident optical power (I_{op}) as it was explained before. In order to estimate η as a function of the excess bias voltage, we use the model presented in [15] as

$$\eta(V_{ex}) = \eta_0 \left(1 - e^{-V_{ex}/V_0}\right). \tag{18}$$

Here, η_0 is a coefficient corresponding to the total detection efficiency saturation value and V_0 represents a normalizing coefficient and are treated as the fitting parameters in our BER model. By total detection efficiency, we mean that the coefficient η includes the SPAD photon detection probability as well as the structure fill-factor.

Accordingly, Fig. 3 compares the experimental data and the estimated BER based on the presented model in this paper and the two fitting parameters obtained as $\eta_0 \simeq 8\%$ and $V_0 \simeq 3$ V. Other (fixed) parameters are given as $n_s = 4$ and $n_{th} = 4$ (indicating the total number of SPADs and the decision threshold), $T_b = 20$ ns corresponding to a bit rate of 50 Mbit/s in the experiment, $T_1 = 12$ ns equal to a duty cycle of 60%, $\Delta = 9$ ns as the measured detector dead time, and $k_{ex} = 200$ denoting the light source extinction ratio. It is worth mentioning that the experiment is conducted according to the setup explained in [6]. Furthermore, at each optical power, the excess bias voltage is varied to achieve the minimum possible BER. Similar optimization is applied in the simulations using the presented model here, where the optimum BER at each optical power is calculated by varying the avalanche trigger probabilities of all parasitics corresponding to different excess bias voltages.

Fig. 3 demonstrates a very good agreement between simulation and measurement and, therefore, we can reliably use the BER model to evaluate the contribution of different parasitics to the BER and identify the bottleneck for further optimizations. This is the major goal of the modeling and analysis presented here, which cannot be met by time-consuming experimental investigation only. To achieve this goal, we perform a traditional sensitivity analysis based on changing one-factor-at-a-time (OFAT) and observing the amount of change in the output which is the minimum achievable BER here. The simulation results are shown in Fig. 4, where the change in the minimum BER is plotted for $\pm 10\%$ of change in the avalanche trigger probabilities of all parasitics including dark-count, afterpulsing, and crosstalk. This result indicates that the crosstalk has the most significant contribution to the BER as compared to the dark-count and afterpulsing effects. Therefore, further improvement can be realized

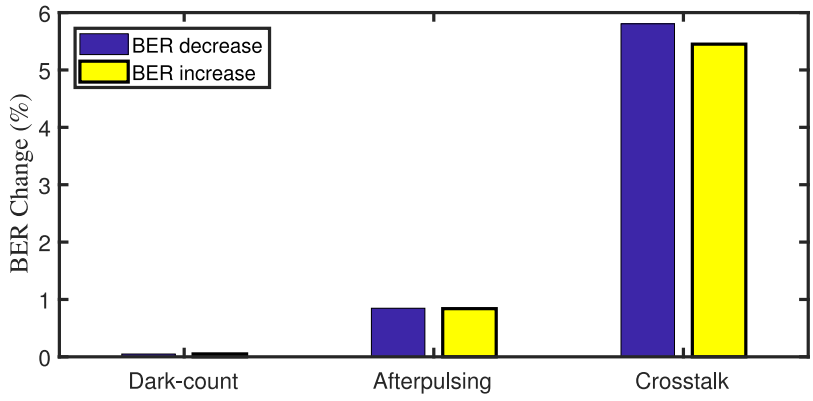

Fig. 4. The change (decrease and increase) in the minimum achievable BER at 50 Mbit/s plotted for (+10% and −10%) change in the avalanche probabilities of parasitics based on the presented BER model and the OFAT sensitivity analysis approach.

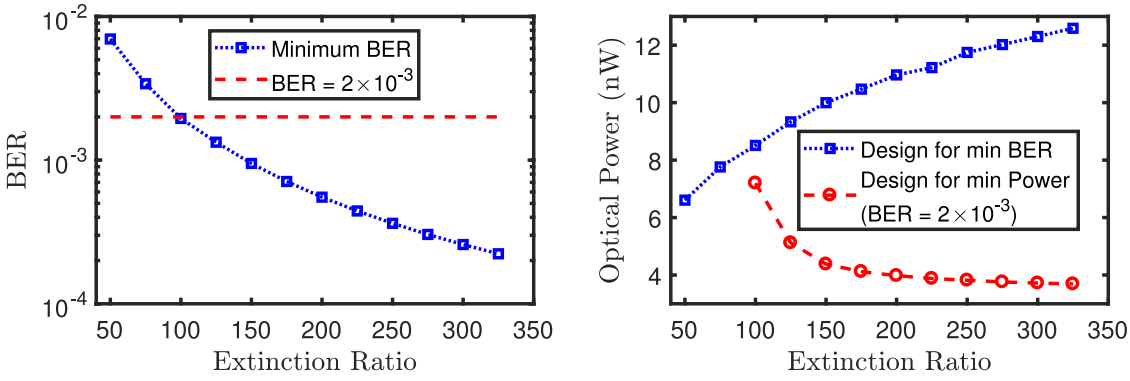

Fig. 5. BER and optical power corresponding to two designs (minimum BER and minimum power) as a function of the light source extinction ratio using the presented model for the 4-SPAD receiver structure at 50 Mbit/s and a digital decision-making with $n_{\text{th}} = 4$.

by reducing the crosstalk. This can be achieved, for example, by increasing the spatial distances between the SPADs, but at the cost of decreased receiver sensitivity. Furthermore, according to the investigations using the model developed here, we predict that if the average one-to-one crosstalk probability is decreased by a factor of 2, a BER of 2×10^{-3} can be obtained using an array of three SPADs with the same detection efficiency, dark-count, and afterpulsing characteristics (i.e. the same 0.35μm PIN-photodiode CMOS technology [6]). This paves the way to further reduce the sensitivity gap to the quantum limit.

Finally, in order to show more clearly how the model presented here can capture the effect of a given parameter on the overall performance, Fig. 5 denotes the BER and the optical power as a function of the light source extinction ratio (k_{ex}) for two different designs. In a first design, the optical power is optimized to achieve the minimum possible BER and in the other design the minimum optical power is calculated corresponding to a given BER (2×10^{-3}). This figure demonstrates that for $k_{\text{ex}} < 100$ it is not possible to obtain a BER smaller than 2×10^{-3} with the 4-SPAD receiver structure. This proves that the optical receiver will be significantly degraded by background light exceeding ~8 nW/100=0.8 nW at which the BER is minimized. This is equivalent to ~5 photons per bit. In addition, the figure shows that at larger extinction ratios less optical power is sufficient to achieve a given BER. However, the power reduction with k_{ex} is not exponential as can be expected according to a first-order BER analysis based on Poissonian photon-counting statistics. This is due to the effect of the parasitics which are properly taken into account in the model presented in this work.

4. Conclusion

BER performance modeling and analysis of a multi-SPAD optical receiver is presented. The model covers all important non-ideality effects including the detector dead time, the light source extinction ratio, and the parasitic effects. It allows more insight into the overall performance and enables the evaluation of the contribution of different parasitics to the BER. It is shown that the crosstalk has the major effect on the BER. Therefore, future work should focus on crosstalk reduction to further improve the performance of the multi-SPAD receivers.

References

[1] P. Hopman, P. Boettcher, L. M. Candell, J. Glettler, R. Shoup, and G. Zogbi, "An end-to-end demonstration of a receiver array based free-space photon counting communications link," in *Proc. Free-Space Laser Commun. VI*, 2006, vol. 6304, Art. no. 63040H.
[2] L. H. Braga *et al.*, "A CMOS mini-SiPM detector with in-pixel data compression for PET applications," in *Proc. Nucl. Sci. Symp. Med. Imag. Conf.*, 2011, pp. 548–552.
[3] D. P. Palubiak and M. J. Deen, "CMOS SPADs: Design issues and research challenges for detectors, circuits, and arrays," *IEEE J. Sel. Topics Quantum Electron.*, vol. 20, no. 6, pp. 409–426, Nov./Dec. 2014.
[4] F. Villa *et al.*, "CMOS imager with 1024 SPADs and TDCs for single-photon timing and 3-D time-of-flight," *IEEE J. Sel. Topics Quantum Electron.*, vol. 20, no. 6, pp. 364–373, Nov./Dec. 2014.
[5] P. Leon *et al.*, "A new underwater optical modem based on highly sensitive Silicon Photomultipliers," in *Proc. OCEANS*, 2017, pp. 1–6.
[6] H. Zimmermann, B. Steindl, M. Hofbauer, and R. Enne, "Integrated fiber optical receiver reducing the gap to the quantum limit," *Sci. Rep.*, vol. 7, no. 1, 2017, Art. no. 2652.
[7] L. Zhang *et al.*, "A comparison of APD-and SPAD-based receivers for visible light communications," *J. Lightw. Technol.*, vol. 36, no. 12, pp. 2435–2442, Jun. 2018.
[8] E. Fisher, I. Underwood, and R. Henderson, "A reconfigurable single-photon-counting integrating receiver for optical communications," *IEEE J. Solid-State Circuits*, vol. 48, no. 7, pp. 1638–1650, Jul. 2013.
[9] D. Chitnis and S. Collins, "A SPAD-based photon detecting system for optical communications," *J. Lightw. Technol.*, vol. 32, no. 10, pp. 2028–2034, May 2014.
[10] H. Mahmoudi, M. Hofbauer, B. Steindl, K. Schneider-Hornstein, and H. Zimmermann, "Statistical study of intrinsic parasitics in a SPAD-based integrated fiber optical receiver," *IEEE Trans. Electron Devices*.
[11] E. Sarbazi, M. Safari, and H. Haas, "Statistical modeling of single-photon avalanche diode receivers for optical wireless communications," *IEEE Trans. Commun.*, vol. 66, no. 9, pp. 4043–4058, Sep. 2018.
[12] A. Spinelli and A. L. Lacaita, "Physics and numerical simulation of single photon avalanche diodes," *IEEE Trans. Electron Devices*, vol. 44, no. 11, pp. 1931–1943, Nov. 1997.
[13] M. A. Karami, "Deep-submicron CMOS single photon detectors and quantum effects," *Ph.D. dissertation, Dept. Elect. Eng., TU Delft, Delft, The Netherlands*, 2011.
[14] C.-C. Chen, "Effect of detector dead time on the performance of optical direct-detection communication links," Jet Propulsion Lab., California Inst. Tech., Pasadena, CA, USA, Tech. Rep. TDA Prog. Rep. 42-93, 1988, pp. 146–154.
[15] V. Savuskan, I. Brouk, M. Javitt, and Y. Nemirovsky, "An estimation of single photon avalanche diode (SPAD) photon detection efficiency (PDE) nonuniformity," *IEEE Sensors J.*, vol. 13, no. 5, pp. 1637–1640, May 2013.